Nano Research
2022, 15(4): 3487–3495

ISSN 1998-0124 CN 11-5974/O4
https://doi.org/10.1007/s12274-021-3902-1

Research Article

Multiplex ratiometric gold nanoprobes based on surface-enhanced Raman scattering enable accurate molecular detection and imaging of bladder cancer

Xiao Liang[1,2,§], Pu Zhang[1,3,§], Minghai Ma[1,§], Tao Yang[1], Xiangwei Zhao[4], Rui Zhang[1], Minxuan Jing[1], Rundong Song[1], Lei Wang[2] (✉), and Jinhai Fan[1] (✉)

[1] *Department of Urology, The First Affiliated Hospital, Xi'an Jiaotong University, Xi'an 710061, China*
[2] *Department of Thoracic Surgery, Tangdu Hospital, Air Force Medical University, Xi'an 710038, China*
[3] *Department of Urology, Zhejiang Provincial People's Hospital, People's Hospital of Hangzhou Medical College, Hangzhou 310014, China*
[4] *State Key Laboratory of Bioelectronics, School of Biological Science and Medical Engineering, National Demonstration Center for Experimental Biomedical Engineering Education, Southeast University, Nanjing 210096, China*
[§] *Xiao Liang, Pu Zhang, and Minghai Ma contributed equally to this work.*

Received: 22 August 2021 / **Revised:** 19 September 2021 / **Accepted:** 22 September 2021

ABSTRACT

Recently, surface-enhanced Raman scattering (SERS) has been successfully used in the non-invasive detection of bladder tumor (BCa). The internal standard method was considered as an effective ratiometric strategy for calibrating signal fluctuation originated from the interference of measurement conditions and samples. However, it is still difficult to detect the target mRNA quantitatively using the current ratiometric SERS nanosensors. In this study, we developed an internal reference based ratiometric SERS assay. Two kinds of molecular beacons (MB) carrying Raman reporter molecules were anchored on sea-urchin-like Au nanoclusters (AuNCs). Thymidine kinase1 (TK1) MBs with hexachlorofluorescein (HEX) were used to capture tumor biomarker TK1 mRNA, and glyceraldehyde 3-phosphate dehydrogenase (GAPDH) MBs with 5(6)-carboxyfluorescein (FAM) were used to offer internal standard signals. The internal reference GAPDH MB can reflect the consistent content of the GAPDH mRNA in single cells. The ratiometric method (I_{745}/I_{645}) can more accurately reflect the content of target mRNA in single cells. The ratiometric nanoprobes had excellent stability (coefficient of variation: 0.3%), high sensitivity (detection limit: 3.4 pM), high specificity (capable of single-base mismatch recognition) and ribozyme-resistant stability. Notably, the nanoprobes can effectively distinguish BCa cells from normal cells, and it was easy to contour the single BCa cell using the ratiometric method. By combining asymmetric polymerase chain reaction (PCR) and ratiometric nanoprobes, it was easy to distinguish the SERS ratio (I_{745}/I_{645}) as low concentration as 10^{-14} M. Further clinical detection in urine samples from patients with BCa confirmed its potential for early noninvasive diagnosis of BCa with the sensitivity of 80% and specificity of 100%, which is superior to the current urine cytological method.

KEYWORDS

surface-enhanced Raman scattering (SERS), internal reference, bladder cancer, non-invasive detection, SERS imaging

1 Introduction

Bladder cancer (BCa) is one of the most common and recrudescent cancer in the world [1, 2]. The golden standard to diagnose BCa is cystoscopy and pathology. However, the cystoscopy is an invasive examination with a sensitivity of 62%–84% [3, 4]. In addition, adverse reactions related to invasive procedures are frequently after cystoscopy [5, 6]. Urine cytology is a non-invasive screening method in clinical practice. But its sensitivity is related with the cancer pathologic grade, ranging only from 4% to 31% [7–10]. Other imaging examination methods, including computed tomography and ultrasonography, are also low-sensitive for detecting early-stage bladder cancer [11–13]. It must be acknowledged that the lack of high-sensitive screening method has affected the diagnosis and prognosis of bladder cancer. Thus, developing a high-sensitive and noninvasive screening method is the key point for BCa in clinical practice.

Surface-enhanced Raman spectroscopy (SERS) can enhance the Raman signals of the target up to 11 orders of magnitude, yielding single molecular level sensitivity and molecular fingerprint specificity [14–17]. SERS has been widely investigated for super-sensitive detection of circulating tumor cells, circulating tumor DNA/RNA, and other biomarkers [18–26]. The classic SERS nanoprobes for detecting RNA or DNA were synthesized with precious metal nanoparticles, molecular beacons (MBs), and stabilizer [27–29]. With the change of conformation, Raman reporter molecules carried by MBs would move away from the nanoparticles, altering the Raman signal. We have previously made the similar SERS nanoprobes to detect epidermal growth factor receptor (EGFR) mutated circulating tumor RNA and free survivin mRNA in urine, winning a high sensitivity of cancer diagnosis [30, 31]. However, the detection process can be easily

Address correspondence to Lei Wang, tuodi1986@126.com; Jinhai Fan, jinhaif029@126.com

interrupted by the poorly reproducible and relatively fluctuating SERS signal because the signal intensity is influenced by many variables, such as working distance, laser power, surface roughness, and even molecular structures. It is difficult to realize quantitative SERS analysis using the traditional nanoprobes [32].

The internal standard (IS) method was considered as an effective ratiometric strategy for calibrating signal fluctuation originated from the interference of measurement conditions and samples [33–35]. It is attractive to develop an IS-based ratiometric SERS assay for quantitative analysis [36]. Many previous studies have demonstrated that the ratiometric SERS nanosensors can provide higher sensitivity, specificity, and reliability [33, 37, 38]. However, the live cell detection of RNA also suffers from cell-to-cell variability arising from target-independent differences, such as cellular uptake of nanoprobes [39, 40]. Accordingly, it is still difficult to detect the target mRNA quantitatively using the current ratiometric SERS nanosensors [41]. Recently, multiplex detection system presented the advantages to allow different RNA targets to be studied concurrently, thereby improving the accuracy of early cancer detection over a single-biomarker assay [42]. In addition, one of the channels can also be utilized as an internal reference for target signal normalization [43].

In previous studies [30, 31, 44–46], we have synthesized sea-urchin-like Au nanoclusters (AuNCs) with abundant nanopricks, sharp protrusions, or crevices, which possessed excellent SERS activity with tremendous enhancement at the "hot spot". In this study, we further developed a novel multiplex ratiometric SERS nanosensor (Fig. 1(a)). The sea-urchin-like AuNCs were produced as SERS substrate, and two kinds of MB carrying Raman reporter molecules were anchored onto AuNCs through Au–S bond. The Thymidine kinase1 (TK1) MBs with hexachlorofluorescein (HEX) can recognized and hybridized with TK1 mRNA which is served as the special biomarker of BCa. Glyceraldehyde 3-phosphate dehydrogenase (GAPDH) mRNA is a housekeeping gene, constantly existing in homologous cells. GAPDH has been widely used as a reference for normalizing other gene expression levels. Thus, GAPDH MBs with 5(6)-carboxyfluorescein (FAM) allowed for cellular GAPDH mRNA levels. The SERS signals of HEX and FAM can be monitored and detected in a single spectrum simultaneously. With dual target detection, the relative expression levels of TK1 can be determined with good accuracy by normalizing their signals against GAPDH mRNA signals as a reference. Furthermore, asymmetric polymerase chain reaction (PCR) was carried out to obtain abundant TK1 single-stranded DNA (ssDNA) in urine samples of 15 patients with BCa (Fig. 1(b)). To explore the potential of the ratiometric SERS nanosensor in clinical practice, the nanosensor was used to diagnose the BCa using the ssDNA in clinical trial.

2 Results and discussion

2.1 Characterization of Au-internal standard MB (ISMB) nanoprobes

Scanning electron microscopy (SEM) and transmission electron microscopy (TEM) showed the special morphology of sea-urchin-like AuNCs (Figs. 2(a) and 2(b)). The AuNCs with a diameter of 120 nm was covered with 79 sharp nanopricks (20 nm length). In our previous study [44, 45], sea-urchin-like AuNCs showed excellent Raman signal enhancement capability. Multiple nanopricks and nanogaps can produce abundant electromagnetic fields and "hot spots" to enhance Raman signals. Enhancement factor (EF) is an objective indicator to measure Raman signal enhancement ability. The EF value of a single AuNCs was estimated to be 3.44×10^7 [30, 31]. Then, the TK1 MB and GAPDH MB were successively coated on the AuNCs to

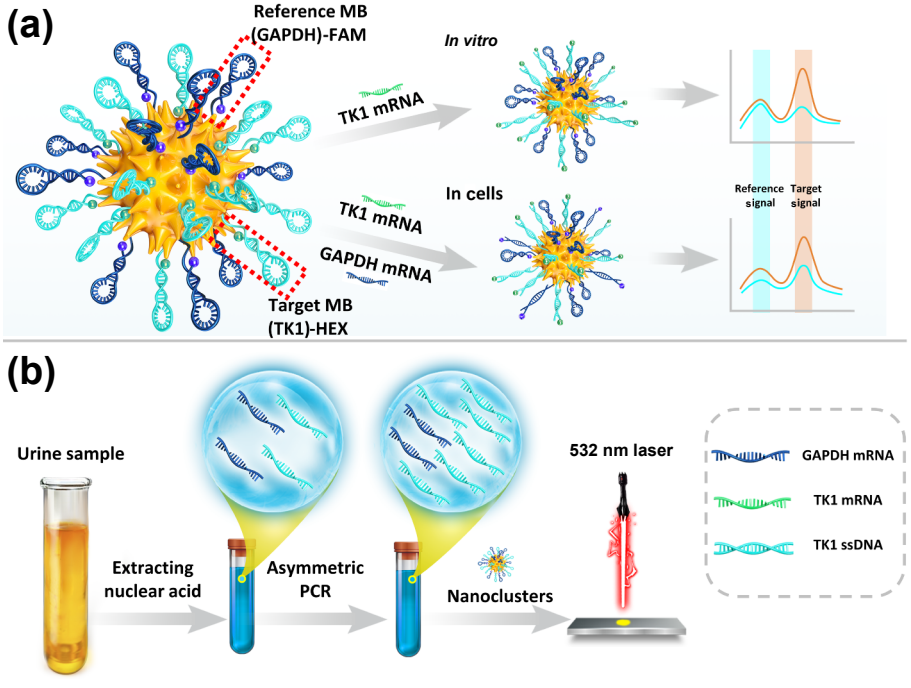

Figure 1 (a) Schematic diagram illustrated the testing principle of multiplex ratiometric gold nanoprobes in cells and outside cells. Two types of MBs are hairpin DNA modified by the Raman reporter molecule HEX or FAM at the 5' end and thiol at the 3' end. In the absence of the target sequences, the MBs acted like a switch, usually partially closed by the stem. At the "off" position, the Raman reporter molecule was located near the surface of AuNCs, and the Raman signal is enhanced due to the surface Raman enhancement effect. After binding with target single stranded nucleic acid outside the cells, the conformational change of TK1 MBs opened the hairpin, making the Raman reporting molecule HEX far away from the surface of AuNCs, and the corresponding Raman signals changed; while the FAM Raman strength would be used as the internal reference signal. In cells, GAPDH MBs would also bind with GAPDH mRNA, changing Raman signal of FAM as a reference signal. (b) Total RNA extracted from urine samples was processed by asymmetric PCR to amplify the target TK1 single strand, and then co-incubated with the nanoprobe for Raman signal detection.

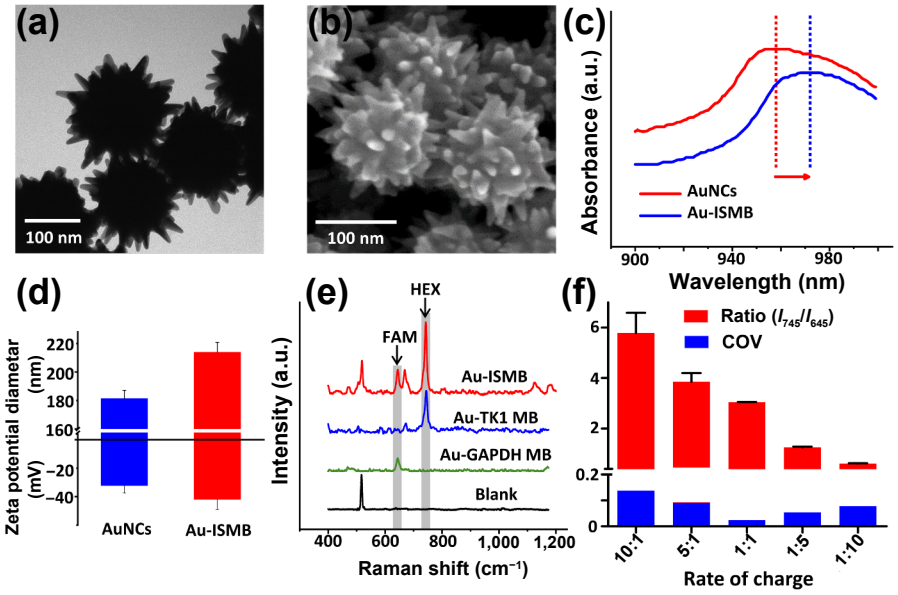

Figure 2 (a) TEM image of AuNCs. (b) SEM image of AuNCs. (c) UV–Vis absorption spectra of AuNCs and Au-ISMB. (d) Hydrodynamic size distribution and Zeta potential of AuNCs and Au-ISMB. (e) The SERS spectra of AuNCs (blank), Au-TK1 MB, Au-GAPDH MB and Au-ISMB, showing that the Raman characteristic peaks of FAM and HEX were at 645 and 745 cm^{-1}. (f) An appropriate ratio of charge can maximize the removing ability of internal reference. The feeding ratios (TK1 MB:GAPDH MB) of different MBs were 10:1, 5:1, 1:1, 1:5 and 1:10.

functionalize the multiplex ratiometric SERS nanosensor. In the whole process of functionalization, the maximum ultraviolet–visible (UV–Vis) absorption peak of red-shifted, moving from 958 to 975 nm (Fig. 2(c)). The average hydrodynamic diameter of nanoparticles increased from 181.3 ± 5.8 to 213.9 ± 6.9 nm, and the Zeta potential decreased from −32.2 ± 5.2 to −41.8 ± 7.3 mV (Fig. 2(d)).

The multiplex ratiometric SERS nanosensor possessed TK1 MB and GAPDH MB. The special SERS spectra of TK1 MB (marked with HEX), GAPDH MB (marked with FAM) and ISMB were compared in Fig. 2(e). The characteristic SERS peaks of HEX were at 745, 1,295, 1,501 and 1,632 cm^{-1}, and the characteristic peaks of FAM were at 469, 645, 1,171, 1,309, 1,431, 1,510 and 1,638 cm^{-1}. More peaks can be detected in the Au-ISMB due to the multiple MB on the nanosensor. It must be worth noting that the characteristic peak at 745 cm^{-1} from HEX and peak at 645 cm^{-1} from FAM can be obviously observed in the complex SERS spectrum of Au-ISMB simultaneously (Fig. 2(e)). The intensities of above two characteristic peaks were used to calculate the SERS ratio (I_{745}/I_{645}) that was set as HEX/FAM.

In order to explore the optimal MB ratio in the coating process, the multiplex nanosensors were fabricated using different feed ratios of ratiometric TK1 to GAPDH MBs (including 10:1, 5:1, 1:1, 1:5, and 1:10). Mapping test defined from the area of 10 μm × 10 μm was performed, as shown in Fig. 1, and the value of I_{745}/I_{645} ratio and coefficient of variation (COV) were used to assess the sensitivity and stability of the SERS signals. As shown in Fig. 2(f), the COV value of I_{745}/I_{645} ratio arrived at a minimum of 0.3% when the feeding ratio of TK1 MB and GAPDH MB was 1:1. That is, the multiplex nanosensors can win the most stable value with the feeding ratio of 1:1. Meanwhile, after drawing the concentration–fluorescence standard curve of the report molecule (Fig. 2), the concentration of coated MBs on the nanometer surface could be calculated and results showed that there was no

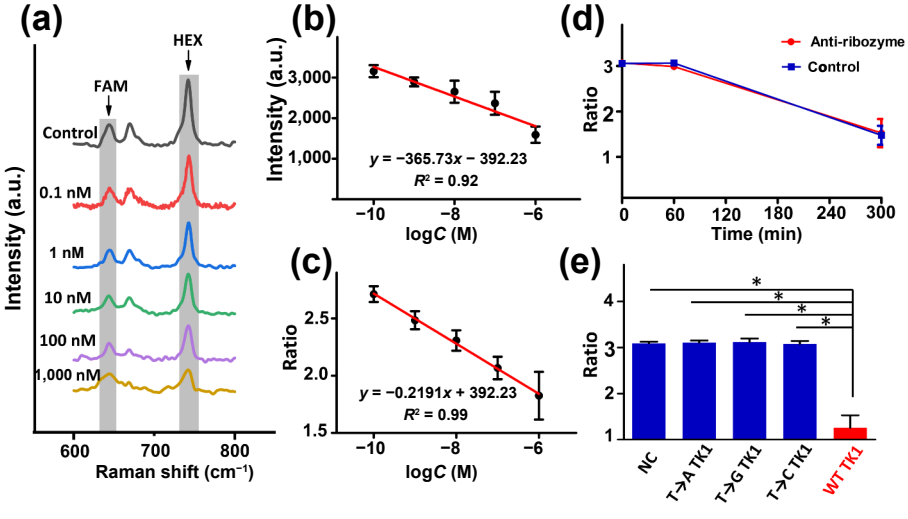

Figure 3 (a) Raman spectra of Au-ISMB in the presence of different concentrations of target sequences. (b) The SERS signal changes of Au-MB (745 cm^{-1}) in the presence of targets sequences with different concentrations. (c) The SERS ratio changes of Au-ISMB (I_{745}/I_{645}) in the presence of targets sequences with different concentrations. (d) Nuclease stability of Au-ISMBG in the presence or absence of DNase I. (e) The SERS ratio changes of Au-ISMB in the presence of mismatch sequence (MS) and target sequence. *$P < 0.01$.

significant difference in different feed ratios (Fig. 3). Thus, feeding ratios of 1:1 was confirmed in the following study. The SERS signals were detected again after the multiplex nanosensors were stored at 4 °C for 30 days. Although the intensity of SERS signals reduced, the I_{745}/I_{645} ratio did not change significantly (Fig. 4). The ratiometric nanosensors had good stability and repeatability in the SERS signals measurement.

2.2 Biochemical properties of Au-ISMB nanoprobes

To evaluate the feasibility of Au-ISMB for detecting mRNA, we conducted a combination study to test the sensitivity, specificity, and nuclease resistance of the nanoprobe. Firstly, Au-ISMB was co-incubated with different concentrations of TK1 target sequences. After annealing processing (reducing the temperature gradually from 95 °C to room temperature at 1 °C/min), the SERS intensity of HEX was reduced significantly, but no SERS signal of FAM changed in the whole process (Fig. 3(a)). The linearity relation between the logarithmic concentration of TK1 mRNA and SERS signal of FAM can be calculated with a low linear correlation coefficient (R^2) of 0.92 (Fig. 3(b)), and the limit of detection (LOD) for TK1 mRNA was calculated to be 3 nM. Remarkably, under the correction of internal reference SERS signal from FAM, the linearity relation between the logarithmic concentration of TK1 mRNA and the ratio of (I_{745}/I_{645}) was improved with a R^2 of 0.99 and the LOD was estimated to be 3.4 pM (Fig. 3(c)). The nanoprobe was efficient for reliably quantitative and sensitive detection of TK1 mRNA, which was attributed to the ratiometric SERS strategy. Nuclease resistance is a key feature of the probe for cell detection. Deoxyribonuclease I (DNase I) is commonly used to evaluate the nuclease resistance of nanoprobes. After being incubated with DNase I for 1 h (experimental group), no significant changes of SERS signals were observed after the ribozyme treatment. Even if being incubated with DNase I and target sequences simultaneously, no SERS signal changes can be observed between the experimental group and the control group. It proved that the nanoprobe had good stability against ribozyme (Fig. 3(d)). To verify the detection specificity of the nanoprobes, Au-ISMB was incubated with ultra-pure water (negative control group), single base mismatch sequence (SBMS), and target sequence under the same conditions, respectively (Fig. 3(e)). The results showed that the nanoprobe can only identify the target TK1 sequence and had good detection specificity.

2.3 Cell experiments of Au-ISMB nanoprobes

In order to verify the ability of Au-ISMB to recognize normal cells and BCa cells, we conducted *in vitro* cell assay experiments, including *in vitro* cell RNA detection and cell Raman imaging. BCa cell lines 5637 and T24 were selected as positive control, while normal fibroblast cell L929 was selected as negative control (NC). Reverse transcription-polymerase chain reaction (RT-PCR) was performed to verify the relative expression of TK1 mRNA in cell lines, using GAPDH as the internal reference. TK1 mRNA was significantly overexpressed in 5637 and T24 cells (Fig. 4(a)). Total RNA was extracted from the three cell lines and the concentration of each RNA was adjusted to 50 ng/μL for co-incubation with nanoprobes, and distillation–distillation H_2O (ddH_2O) was selected as NC group (Fig. 4(b)). After being incubated with total RNA of 5637 and T24 cells, the I_{745}/I_{645} ratio reduced significantly (Fig. 5). The I_{745}/I_{645} ratio of L929 cells was higher than that of the NC group. The specific data can be found in Fig. 6(b). As GAPDH mRNA expression is stable both in normal epithelial cells and tumor cells, the Raman signal of FAM at 645 cm^{-1} showed a similar decline in all cells. However, the Raman signals of HEX at 745 cm^{-1} in L929 group did not decrease significantly due to the trace expression of TK1 mRNA. As a result, I_{745}/I_{645} in L929 group was higher than that in NC.

For further biological application of Au-ISMB nanoprobes in live cells imaging, 3-(4,5-dimethylthiazol-2-yl)-2,5-

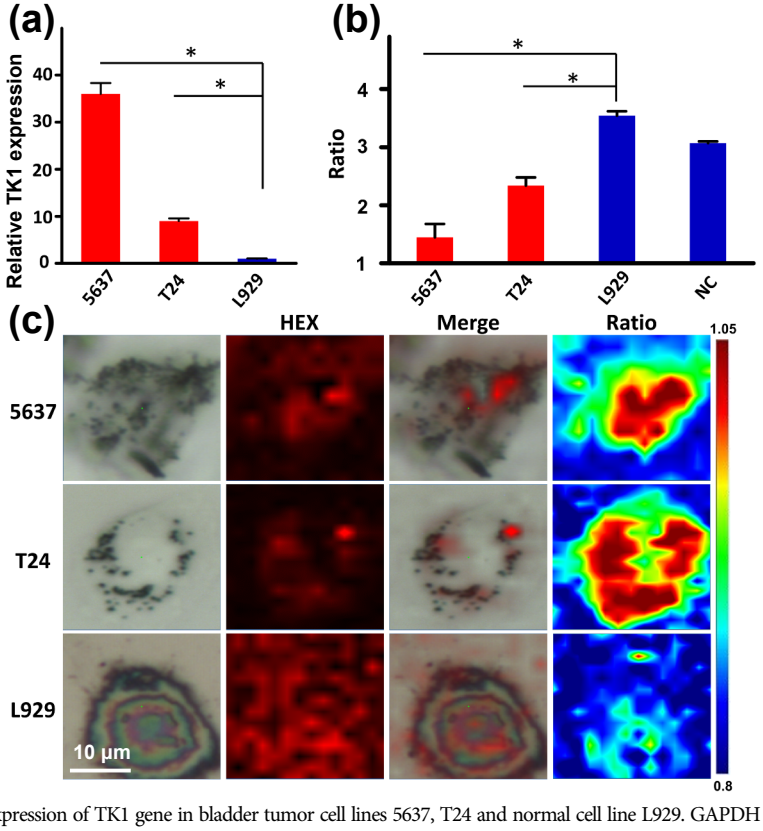

Figure 4 (a) The relative DNA expression of TK1 gene in bladder tumor cell lines 5637, T24 and normal cell line L929. GAPDH was used as intracellular reference. (b) The SERS ratio changes of Au-ISMB nanosensors after co-incubation of total RNA. ddH_2O was used as a negative control. (c) Single cell Raman mapping imaging dependent on HEX signal intensity and SERS ratio (I_{645}/I_{745}). *$P < 0.01$.

diphenyltetrazolium bromide (MTT) assays were carried out to test the cytotoxicity of nanoprobes. The cell viability always stayed above 90% after being incubated with the nanoprobes at a concentration of 200 μg/mL for 48 h (Fig. 6). Low cytotoxicity of the nanoprobes is the foundation for the next living cell imaging. In single cell SERS mapping study, the overlay image of the bright-field image showed that the nanoprobes were taken up into the cells. It was difficult to contour the cancer cells only using the SERS signals of HEX. Also, it cannot distinguish normal cells and BCa cells using the SERS signals of HEX. Furthermore, the contour of single T24 or 5637 cells could be clearly depicted once the I_{745}/I_{645} ratio was used (Fig. 4(c)). It is easy to identify the BCa cells and normal cells obviously based on the ratiometric method. Herein, the internal reference signal from GAPDH MB played a significant role in tumor cell detection and imaging. The GAPDH gene is consistently expressed in almost all cells and is recognized as a reliable intracellular reference in PCR and western blot experiment. The GAPDH MB on the nanoprobes opened consistently in all BCa cells, and the SERS intensity at 645 cm^{-1} can reflect the content of the GAPDH mRNA in single cells. Thus, the ratiometric method (I_{745}/I_{645}) can more accurately reflect the content of target mRNA in single cells.

2.4 Super-sensitive detection of TK1 mRNA in cells and clinical samples

In order to improve the detection sensitivity of the Au-ISMB nanoprobes, asymmetric PCR was applied to obtain abundant ssDNA before the clinical experiment. A series of experiments were conducted to verify the improvement of detection performance with asymmetric PCR. In the two-step asymmetric PCR, the TK1 double-stranded DNA of BCa cells was amplified in the first step, and then the target ssDNA matched with TK1 MB was amplified in the second step by the asymmetric primer concentration method. The ssDNA with half molecular weight after the two-step asymmetric PCR was observed in the gel electrophoresis experiment. No electrophoresis bands generated by nonspecific amplification could be observed (Fig. 5(a)). Sequencing of the product further proved that the target ssDNA was successfully obtained and could be recognized by the Au-ISMB nanoprobes (Table S1 in the Electronic Supplementary Material (ESM)). Firstly, the synthetic TK1 target sequences by gradient concentration were used to test the sensitivity of Au-ISMB nanoprobes and asymmetric PCR. The corresponding asymmetric PCR electrophoretic band and SERS ratio (I_{745}/I_{645}) were shown in Fig. 5(b), and the minimum detected concentration of TK1 target sequences reached 0.01 pM using SERS ratio (I_{745} /I_{645}). Next, the total mRNA extracted from 5637 cells was diluted by gradient concentration. As shown in Fig. 5(c), it was easy to distinguish the SERS ratio (I_{745}/I_{645}) as low concentration as 0.1 ng/μL. Therefore, the minimum tumor cell RNA load was calculated as 2 ng. The asymmetric PCR could effectively amplify abundant target ssDNA to improve the detection ability of Au-ISMB nanoprobes. Noteworthily, asymmetric PCR protocols require extensive optimization to reduce the production of nonspecific amplification. Meanwhile, PCR mixtures could reduce the stability of the nanoprobes, and the products must be purified before detection by the nanoprobe.

In this study, 15 patients with pathologically confirmed BCa (Table 1) and 7 healthy people were included. The total RNA was extracted from the urine samples. After asymmetric PCR experiment, the products were co-incubated and annealed with Au-ISMB. The SERS ratio (I_{745}/I_{645}) from healthy people and patients showed significant differences (Fig. 6(a)). It is easy to identify the cancerous samples using the SERS ratio. Meanwhile, RT-PCR was used as the gold standard to confirm the expression of TK1 mRNA in the corresponding BCa tissues (Fig. 6(b)). TK1 mRNA was highly expressed in 13 patients with an expressive rate of 86.7% (13/15). Thus, the sensitivity to detect TK1 mRNA in urine samples was 92.3% (12/13). In total, the sensitivity and specificity to detect BCa in urine samples were 80% (12/15) and 100% (7/7). This method was more effective than current urinary cytology tests in clinical practice.

3 Conclusions

In this study, we developed an internal reference based ratiometric SERS assay. The internal reference GAPDH MB can reflect the consistent content of the GAPDH mRNA in single cells. The ratiometric method (I_{745}/I_{645}) can more accurately reflect the content of target mRNA in single cells. The Au-ISMB nanoprobes have excellent detection sensitivity (threshold: 3.4 pM) and stability with a COV of 0.3%. Notably, the nanoprobes can effectively distinguish BCa cells from normal cells, and it is easy to contour the single BCa cell using the ratiometric method. To increase the detection accuracy in clinical application, asymmetric PCR was carried out to produce abundant target ssDNA. The combination of asymmetric PCR and IS-based ratiometric SERS assay had a higher detection ability, and the minimum detection concentration of target RNA reached 0.01 pM. Further clinical detection in urine samples from patients with BCa confirmed its potential for early noninvasive diagnosis of BCa with the

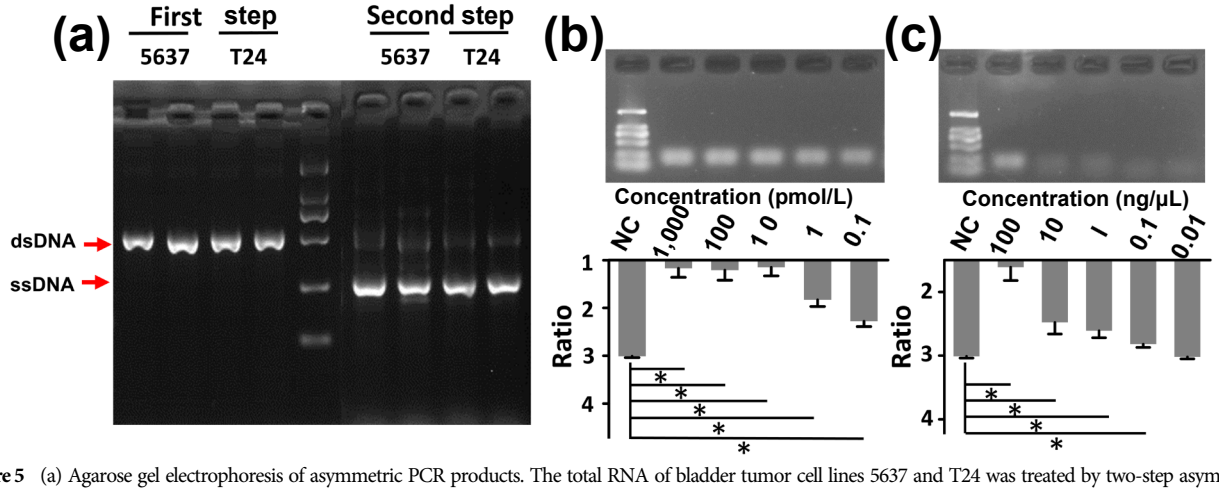

Figure 5 (a) Agarose gel electrophoresis of asymmetric PCR products. The total RNA of bladder tumor cell lines 5637 and T24 was treated by two-step asymmetric PCR. (b) Changes of SERS ratio of Au-ISMB after co-incubating with the synthetic target sequences with different concentrations. (c) Changes of SERS ratio of Au-ISMB after co-incubating with the ssDNA of asymmetric PCR which were obtained using total RNA in urine samples. *$P < 0.01$.

Table 1 Clinical characteristics of patients with bladder tumor

Patient number	Age/sex	TNM staging	Grade
1	55/M[a]	$T_1N_0M_0$	Low
2	68/M	$T_1N_0M_0$	High
3	74/F[b]	$T_1N_0M_0$	High
4	58/M	$T_1N_0M_0$	High
5	72/F	$T_1N_0M_0$	Low
6	61/M	$T_1N_0M_0$	High
7	53/F	$T_1N_0M_0$	High
8	65/F	$T_1N_0M_0$	Low
9	43/F	$T_1N_0M_0$	High
10	66/M	$T_1N_0M_0$	High
11	52/F	$T_1N_0M_0$	High
12	73/F	$T_1N_0M_0$	High
13	64/F	$T_1N_0M_0$	Low
14	57/M	$T_1N_0M_0$	High
15	53/F	$T_1N_0M_0$	High

[a]F refers to female, and [b]M means male.

sensitivity of 80% and specificity of 100%, which is superior to the current urine cytological method.

4 Experimental section

4.1 Reagents and materials

DNA oligonucleotides were synthesized and purified by Shanghai Sangon Biotechnology. The sequence of oligonucleotides was shown in Table 2. Hydrogen tetrachloroaurate(III) ($HAuCl_4{\cdot}4H_2O$), $AgNO_3$, tris(2-carboxylethyl)phosphine hydrochloride (TCEP·HCl), glycerin, levodopa (L-DOPA), and red blood cell (RBC) lysis buffers were purchased from Sigma Chemical Company (St. Louis, USA); trisodium citrate ($C_6H_5Na_3O_7{\cdot}2H_2O$), mercaptoethanol (ME), sodium dodecyl sulfate (SDS), NaH_2PO_4, and NaCl were purchased from China National Pharmaceutical Group Co. (Shanghai, China); mercapto polyethylene glycol (PEG-SH, 5,000 DA) was purchased from JenKem Technology Co. (Beijing, China); DNase I and SYBR Green Master Mix were purchased from Takara Biotechnology Company (Dalian, China); Trizol reagent was purchased from Thermo Fisher Scientific; culture products were purchased from Life Technologies Co. (Carlsbad, USA). All chemicals were analytical grade and were used without further purification. Ultra-pure water was used throughout the experiment. Human bladder cancer 5637 and T24 cell lines were provided by Dr. Leland W. K. Chung (CedarsSinai Medical Center, Los Angeles, CA, USA), Normal fibroblasts (cell line name: L929) were purchased from Center for Excellence in Molecular Cell Science, Chinese Academy of Sciences (CAS) (Shanghai, China).

4.2 Preparation of AuNCs probes

The sea-urchin like AuNCs was synthesized by seed-mediated growth [30, 31, 44–47]. Firstly, seed Ag nanoparticles with a diameter of about 30 nm were synthesized. The mixture of glycerol and ultrapure water (7:3) was heated to 95 °C and stirred for 10 min. Then, 2 mL $AgNO_3$ (9 mg/mL) and 10 mL trisodium citrate (10 mg/mL) were added into the mixture successively. The reaction lasted for 1 h at 95 °C. After the mixture was cooled to room temperature, the silver seeds were separated and centrifuged (12,000 rpm, 12 min). 7.2 mL of $HAuCl_4$ (10 mm) was mixed with 12.8 mL of ultra-pure water and heat to 15 °C (300 rpm, 10 min). Then 1 mL of seed Ag nanoparticles and 7.2 mL of L-DOPA (10 mM) were added. The colour of the mixture changed from light yellow to dark brown. The reaction required stirring at 100 rpm for 10 min. The AuNCs were separated from the mixture, centrifuged (6,000 rpm, 1 min) and then washed with formic acid, ammonium hydroxide, and ultra-pure water in sequence. The prepared AuNCs (10^{-13} M) and MBs (10^{-7} M) were mixed and shaken for 4 h. Then 0.1% SDS solution and 0.1 M phosphate buffer (pH 7.4) were added to achieve a concentration of 1/10 of the original concentration of both reagents. After the solution was incubated for more than 10 h, 0.1 M NaCl solution was added, stirred continuously for more than 4 h, and centrifuged at 6,000 rpm for 1 min. The poly(ethylene glycol) methyl ether thiol (mPEG-SH) was then added to the suspension to fill the areas not covered by MBs. Then, it was suspended again in ultrapure water.

4.3 Physicochemical characterization of AuNCs probes

The morphology of all nanoparticles was observed by SEM (model S4800; Hitachi Ltd., Tokyo, Japan) and TEM (Model H7650; Hitachi Ltd., Tokyo, Japan). UV–Vis absorption spectra were

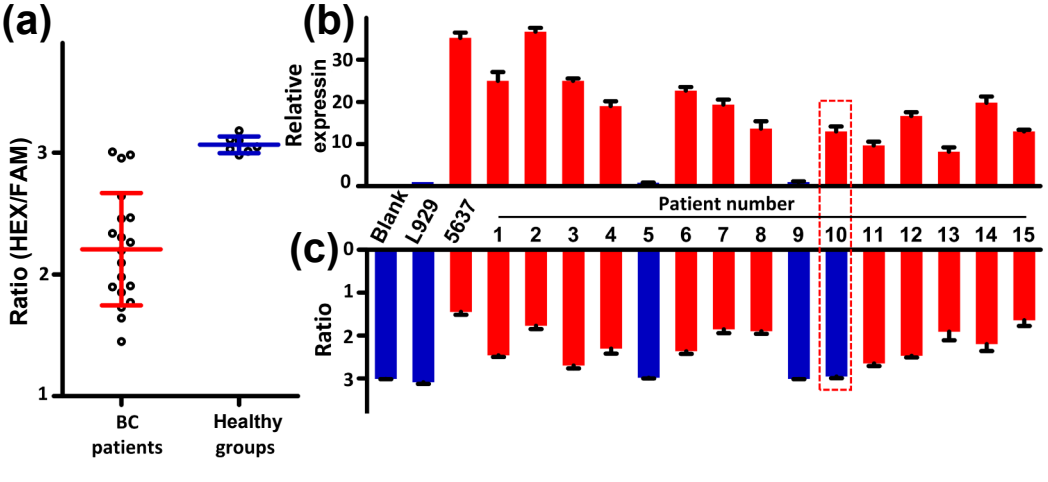

Figure 6 (a) The SERS ratio of urine samples in normal population and patients with bladder tumor. Total RNA was extracted from urine samples and amplified using asymmetric PCR. The products were co-incubated with Au-ISMB. (b) Relative expression level of TK1 mRNA in tumor tissues. ddH_2O, mRNA of L929 and mRNA of 5637 were used as blank control, negative control and positive control respectively. (c) The SERS ratio after co-incubating with the asymmetric PCR products of patients' urine samples. Blue column indicates no difference between the signal and blank or negative control, and red column indicates the difference between the signal and blank or negative control. The expression of TK1 in tumor tissue of patients did not match the SERS ratio of urine samples.

Table 2 Sequences of oligonucleotides used in this study

Name	Sequence
TK1 MB	5'HEX-ACGACGCCAGGGAGAACAGAAACCGTCGT-3'SH
GAPDH MB	5'FAM-CGACGGAGTCCTTCCACGATACCACGTCG-3'SH
Target sequence	5'-GTTTCTGTTCTCCCTGG -3'
Single-base(A) MS	5'-GTTTCTGTACTCCCTGG -3'
Single-base(G) MS	5'-GTTTCTGTGCTCCCTGG -3'
Single-base(C) MS	5'-GTTTCTGTCCTCCCTGG -3'
The primer of TK1 mRNA, forward	5'-TATGCCAAAGACACTCGCTAC-3'
The primer of TK1 mRNA, reverse	5' -GCAGAACTCCACGATGTCAG -3'
The primer of GAPDH mRNA, forward	5'-CTAGGCCACAGAATTGAAAGATCT-3'
The primer of GAPDH mRNA, reverse	5'-GTAGGTGGAAATTCTAGCATCATCC-3'
Forward primer for asymmertric PCR	5'- CGGCTTTCACTGCTGAGTTTC -3'
Reverse primer for asymmertric PCR	5'- AAGGAAACAAGAGGGCGTGA -3'
The template sequence for asymmertric PCR	5'-CGCTGTTGACATCAGCCTGCTTCTTCCCCTCTGCGGCTTTCACTGCTGAGT TTCTGTTCTCCCTGGGAAGCCTGTGCCAGCACCTTTGAGCCTTGGCCCAC ACTGAGGCTTAGGCCTCTCTGCCTGGGATGGGCTCCCACCCTCCCCTGAG GATGGCCTGGATTCACGCCCTCTTGTTTCCTTTTGGG -3'

detected (Beckman DU800; Beckman Coulter Inc., Atlanta, USA). A Zeta-sizer (Malvern Zeta sizer; Malvern Ins. Ltd., Malvern, UK) was used to analyze the size distribution and Zeta potential in water at 25 °C. SERS spectra were obtained by a laser Raman spectrometer (LabRAM HR800; HORIBA Ltd., Paris, France). The laser radiation was 532 nm; the acquisition time was 10 s, and the laser power on the sample surface was 0.710 mW.

4.4 Quantitation of MBs loaded on the nanoprobe

The ME (final concentration 20 mM) was added to the probe solution. The mixture was shaken violently overnight at room temperature to release modified molecular beacons. The molecular beacons in the supernatant were obtained by centrifugation (4,000*g*, 5 min). Then, a multi-mode microplate reader (SynergyMx; Bio-Tek Instruments Inc., Winooski, USA) was used to measure the fluorescence in the supernatant. The fluorescence of HEX was excited at 535 nm and measured at 553 nm. The fluorescence of the FAM was excited at 495 nm and measured at 521 nm.

4.5 Hybridization experiment

To test the specificity of the nanoprobes, AuNCs nanosensors were incubated with single base mismatch sequence and target sequence. To test the sensitivity of the nanoprobes, AuNCs nanosensors were incubated with the target sequence at a concentration gradient (0, 0.1, 1, 10, 10, and 1,000 nM). To evaluate the stability of the AuNCs probe, DNase I (0.02 U/mL) and targeted sequence were successively added into the mixture. SERS signals were obtained under the excitation of a 532 nm laser.

4.6 Cell culture

5637 cell lines were cultured in RMI-1640 culture medium, while T24 and L929 cell lines were cultured in Dulbecco's modified Eagle medium (DMEM). All cell lines were supplemented with 10% fetal bovine serum (FBS) and 100 U/mL 1% penicillin/streptomycin. The cells were kept at a 37 °C and 100% humidified incubator containing 5% CO_2.

4.7 PCR and asymmetric PCR procedure

Total RNA was extracted from the cells using Trizol reagent according to the manufacturer's protocol. Complementary DNA (cDNA) was then synthesized using the Primerscript RT kit. In addition, the relative levels of the target gene transcript were measured using RT-PCR (C1000 Thermal Cycler; Bio-Rad Laboratories Inc.). All the experiments were repeated for three times. GAPDH cDNA was amplified as an internal control. The asymmetric PCR reaction was divided into two steps. The first step was the same as the above method. In the second step reaction, each 30 μL reaction volume consisted of 12 μL free nuclease water, 15 μL 2× Taq PCR Mastermix (Hangzhou Baosai Biotechnology Co., Ltd., PM06), 2 μL forward primers (Table 1, 100 μM) and 0.5 μL first step PCR reaction product. PCR amplification was performed under the following conditions: 95 °C for 5 min, followed by 35 cycles of PCR at 95 °C for 30 s, 55 °C for 30 s, 72 °C for 40 s, and then finally extended for 7 min at 72 °C. Finally, PCR reaction buffer was diluted to 100 μL at 25 °C and stored at 4 °C for using. Asymmetric PCR products were analyzed by agarose gel electrophoresis. The gel concentration was 1%; the voltage was 100 V, and the electrophoresis time was 30 min. The ssDNA bands of the corresponding agarose gel were then removed. ssDNA was extracted from the agarose gel using GenElute™ Gel Extraction Kit (Sigma-Aldrich Corporation, USA).

4.8 Cell Raman mapping imaging

Before SERS mapping, the cells were incubated with AuNCs for 4 h and washed 3 times with phosphate-buffered saline (PBS) to remove the medium and free particles, and then SERS mapping was performed on the cells. The characteristic Raman band of HEX in 740–750 cm^{-1} and the ratio of I_{745}/I_{645} were selected to establish SERS images. The objective lens (50× telephoto lens) and 532 nm laser were selected, and the excitation beam was quasi sized to a spot of ~ 1 μm^2. A *X*-*Y* platform controlled by computer was used to carry out rasterization scanning on the cells, to obtain the laser induced spectrum (mainly SERS and autofluorescence background) for each pixel in the region of interest.

4.9 Urine specimen

The urine samples were collected from the Department of Urology, the First Affiliated Hospital of Xi'an Jiaotong University. The research programme was approved by the Institutional Review Committee of the First Affiliated Hospital of Xi'an Jiaotong University School of Medicine (Xi'an, China) and was carried out in accordance with the Helsinki Declaration. Urine samples were collected from patients diagnosed with bladder

cancer and centrifuged (1,000*g*, 10 min) to separate the exfoliated cell. The erythrocyte was removed from the cell ball with erythrocyte lysis buffer. It was then immediately processed after using the kit RNA extraction reagent according to manufacturer's protocol, and the RNA samples were further purified using a cleaning tool and stored at −80 ℃. The RNA sample was adjusted to the same concentration of a normalized marker. The RNA samples were further used for asymmetric PCR process. Then the product was incubated with the nanoprobes, and SERS signals were stimulated at an appropriate wavelength.

4.10 Data analysis

Raman signals were collected by a laser confocal microscope, and the data of Raman spectra were analyzed by LabSpec software. 8 spectra were collected from each specimen for this study. The first order Savitsky-Golay filter (7 points) was used to preprocess the original spectrum and smooth the noise. Then, the fifth order polynomial was used to fit the baseline, and the smoothed spectral line data were subtracted from the baseline data to obtain the final Raman spectral signal. Student's *t* test was used to compare the SERS intensity between different groups. *P* values of < 0.05 was significant.

Acknowledgements

This work was supported by the National Natural Science Foundation of China (No. 81901838), the Key Research and Development Plan in Shaanxi Province (Nos. 2020SF-123 and 2020SF-195), the Natural Science Foundation of Zhejiang Province (No. LQ21H160041), and the Medical Research Program of Department of Science and Technology of Xi'an, Shaanxi Province (No. 2019115713YX012SF048(4)). We thank Mengzhao Zhang, Qiuya Shao, Lu Wang and Lu Zhang at Department of Urology, the First Affiliated Hospital, Xi'an Jiaotong University for their support. We also thank Dr. Yu Wang at Instrument Analysis Center of Xi'an Jiaotong University for her assistance.

Electronic Supplementary Material: Supplementary material (expanded sequencing of asymmetric PCR products, mapping test of Au-ISMB, the standard curve, the detailed information of optimizing the feeding ratios, stability study of Au-ISMB, cytotoxicity of Au-ISMB, and the detailed information of cancer cells detection ability) is available in the online version of this article at https://doi.org/10.1007/s12274-021-3902-1.

References

[1] Burger, M.; Catto, J. W. F.; Dalbagni, G.; Grossman, H. B.; Herr, H.; Karakiewicz, P.; Kassouf, W.; Kiemeney, L. A.; La Vecchia, C.; Shariat, S. et al. Epidemiology and risk factors of urothelial bladder cancer. *Eur. Urol.* **2013**, *63*, 234–241.

[2] Siegel, R. L.; Miller, K. D.; Jemal, A. Cancer statistics, 2018. *CA: Cancer J. Clin.* **2018**, *68*, 7–30.

[3] Jocham, D.; Stepp, H.; Waidelich, R. Photodynamic diagnosis in urology: State-of-the-art. *Eur. Urol.* **2008**, *53*, 1138–1150.

[4] Bray, F.; Ferlay, J.; Soerjomataram, I.; Siegel, R. L.; Torre, L. A.; Jemal, A. Global cancer statistics 2018: GLOBOCAN estimates of incidence and mortality worldwide for 36 cancers in 185 countries. *CA: Cancer J. Clin.* **2018**, *68*, 394–424.

[5] Biardeau, X.; Lam, O.; Ba, V.; Campeau, L.; Corcos, J. Prospective evaluation of anxiety, pain, and embarrassment associated with cystoscopy and urodynamic testing in clinical practice. *Can. Urol. Assoc. J.* **2017**, *11*, 104–110.

[6] Burke, D. M.; Shackley, D. C.; O'Reilly, P. H. The community-based morbidity of flexible cystoscopy. *BJU Int.* **2002**, *89*, 347–349.

[7] Têtu, B. Diagnosis of urothelial carcinoma from urine. *Mod. Pathol.* **2009**, *22 Suppl 2*, S53–S59.

[8] Lotan, Y.; Roehrborn, C. G. Sensitivity and specificity of commonly available bladder tumor markers versus cytology: Results of a comprehensive literature review and meta-analyses. *Urology* **2003**, *61*, 109–118.

[9] Raitanen, M. P.; Aine, R.; Rintala, E.; Kallio, J.; Rajala, P.; Juusela, H.; Tammela, T. L. J.; Group, F. Differences between local and review urinary cytology in diagnosis of bladder cancer. An interobserver multicenter analysis. *Eur. Urol.* **2002**, *41*, 284–289.

[10] Mowatt, G.; Zhu, S.; Kilonzo, M.; Boachie, C.; Fraser, C.; Griffiths, T. R. L.; N'Dow, J.; Nabi, G.; Cook, J.; Vale, L. Systematic review of the clinical effectiveness and cost-effectiveness of photodynamic diagnosis and urine biomarkers (FISH, ImmunoCyt, NMP22) and cytology for the detection and follow-up of bladder cancer. *Health Technol. Assess.* **2010**, *14*, 1–331.

[11] Usuba, W.; Urabe, F.; Yamamoto, Y.; Matsuzaki, J.; Sasaki, H.; Ichikawa, M.; Takizawa, S.; Aoki, Y.; Niida, S.; Kato, K. et al. Circulating miRNA panels for specific and early detection in bladder cancer. *Cancer Sci.* **2019**, *110*, 408–419.

[12] Dudley, J. C.; Schroers-Martin, J.; Lazzareschi, D. V.; Shi, W. Y.; Chen, S. B.; Esfahani, M. S.; Trivedi, D.; Chabon, J. J.; Chaudhuri, A. A.; Stehr, H. et al. Detection and surveillance of bladder cancer using urine tumor DNA. *Cancer Discov.* **2019**, *9*, 500–509.

[13] Ma, M. H.; Zhang, P.; Liang, X.; Cui, D. X.; Shao, Q. Y.; Zhang, H. B.; Zhang, M. Z.; Yang, T.; Wang, L.; Zhang, N. et al. R11 peptides can promote the molecular imaging of spherical nucleic acids for bladder cancer margin identification. *Nano Res.*, in press, http://doi.org/10.1007/s12274-021-3807-z.

[14] Akkilic, N.; Geschwindner, S.; Höök, F. Single-molecule biosensors: Recent advances and applications. *Biosens. Bioelectron.* **2020**, *151*, 111944.

[15] Pallaoro, A.; Mirsafavi, R. Y.; Culp, W. T. N.; Braun, G. B.; Meinhart, C. D.; Moskovits, M. Screening for canine transitional cell carcinoma (TCC) by SERS-based quantitative urine cytology. *Nanomedicine: Nanotechnol., Biol. Med.* **2018**, *14*, 1279–1287.

[16] Shao, X. G.; Pan, J. H.; Wang, Y. Q.; Zhu, Y. J.; Xu, F.; Shangguan, X.; Dong, B. J.; Sha, J. J.; Chen, N.; Chen, Z. Y. et al. Evaluation of expressed prostatic secretion and serum using surface-enhanced Raman spectroscopy for the noninvasive detection of prostate cancer, a preliminary study. *Nanomedicine: Nanotechnol., Biol. Med.* **2017**, *13*, 1051–1059.

[17] Liu, Y. S.; Luo, F. Spatial Raman mapping investigation of SERS performance related to localized surface plasmons. *Nano Res.* **2020**, *13*, 138–144.

[18] Ngo, H. T.; Wang, H. N.; Fales, A. M.; Vo-Dinh, T. Plasmonic SERS biosensing nanochips for DNA detection. *Anal. Bioanal. Chem.* **2016**, *408*, 1773–1781.

[19] Kneipp, K.; Kneipp, H.; Kneipp, J. Surface-enhanced Raman scattering in local optical fields of silver and gold nanoaggregates-from single-molecule Raman spectroscopy to ultrasensitive probing in live cells. *Acc. Chem. Res.* **2006**, *39*, 443–450.

[20] Pang, Y. F.; Wang, C. G.; Lu, L. C.; Wang, C. W.; Sun, Z. W.; Xiao, R. Dual-SERS biosensor for one-step detection of microRNAs in exosome and residual plasma of blood samples for diagnosing pancreatic cancer. *Biosens. Bioelectron.* **2019**, *130*, 204–213.

[21] Lin, D.; Wu, Q.; Qiu, S. F.; Chen, G. N.; Feng, S. Y.; Chen, R.; Zeng, H. S. Label-free liquid biopsy based on blood circulating DNA detection using SERS-based nanotechnology for nasopharyngeal cancer screening. *Nanomedicine: Nanotechnol., Biol. Med.* **2019**, *22*, 102100.

[22] Restaino, S. M.; White, I. M. Real-time multiplexed PCR using surface enhanced Raman spectroscopy in a thermoplastic chip. *Lab Chip* **2018**, *18*, 832–839.

[23] Peng, R. Y.; Si, Y. M.; Deng, T.; Zheng, J.; Li, J. S.; Yang, R. H.; Tan, W. H. A novel SERS nanoprobe for the ratiometric imaging of hydrogen peroxide in living cells. *Chem. Commun.* **2016**, *52*, 8553–8556.

[24] Liu, W.; Li, W. T.; Li, Y. H.; Li, J. F.; Bai, H.; Zou, M. Q.; Xi, G. C. Determine the position of nanoparticles in cells by using surface-enhanced Raman three-dimensional imaging. *Nano Res.* **2021**, in press, https://doi.org/10.1007/s12274-021-3726-z.

[25] Faulds, K.; Smith, W. E.; Graham, D. Evaluation of surface-

enhanced resonance Raman scattering for quantitative DNA analysis. *Anal. Chem.* **2004**, *76*, 412–417.

[26] Fan, S. S.; Cheng, J.; Liu, Y.; Wang, D. F.; Luo, T.; Dai, B.; Zhang, C.; Cui, D. X.; Ke, Y. G.; Song, J. Proximity-induced pattern operations in reconfigurable DNA origami Domino array. *J. Am. Chem. Soc.* **2020**, *142*, 14566–14573.

[27] Li, Y. E.; Wang, Z.; Mu, X. J.; Ma, A. N.; Guo, S. Raman tags: Novel optical probes for intracellular sensing and imaging. *Biotechnol. Adv.* **2017**, *35*, 168–177.

[28] Qian, X. M.; Zhou, X.; Nie, S. M. Surface-enhanced Raman nanoparticle beacons based on bioconjugated gold nanocrystals and long range plasmonic coupling. *J. Am. Chem. Soc.* **2008**, *130*, 14934–14935.

[29] Ren, L. J.; Chen, X. X.; Feng, C.; Ding, L.; Liu, X. M.; Chen, T. S.; Zhang, F.; Li, Y. L.; Ma, Z. L.; Tian, B. et al. Visualized and cascade-enhanced gene silencing by smart DNAzyme-graphene nanocomplex. *Nano Res.* **2020**, *13*, 2165–2174.

[30] Guo, T.; Li, W. M.; Qian, L.; Yan, X. L.; Cui, D. X.; Zhao, J. B.; Ni, H. B.; Zhao, X. W.; Zhang, Z. P.; Li, X. F. et al. Highly-selective detection of EGFR mutation gene in lung cancer based on surface enhanced Raman spectroscopy and asymmetric PCR. *J. Pharmaceut. Biomed. Anal.* **2020**, *190*, 113522.

[31] Zhang, P.; Zhang, Y. N.; Liu, W. H.; Cui, D. X.; Zhao, X. W.; Song, J.; Guo, T.; Ni, H. B.; Zhang, M. Z.; Zhang, H. B. et al. A molecular beacon based surface-enhanced Raman scattering nanotag for noninvasive diagnosis of bladder cancer. *J. Biomed. Nanotechnol.* **2019**, *15*, 1589–1597.

[32] Meng, X. Y.; Wang, H. Y.; Chen, N.; Ding, P.; Shi, H. Y.; Zhai, X.; Su, Y. Y.; He, Y. A graphene-silver nanoparticle-silicon sandwich SERS chip for quantitative detection of molecules and capture, discrimination, and inactivation of bacteria. *Anal. Chem.* **2018**, *90*, 5646–5653.

[33] Zhang, Y.; Yan, Y. R.; Chen, W. H.; Cheng, W.; Li, S. Q.; Ding, X. J.; Li, D. D.; Wang, H.; Ju, H. X.; Ding, S. J. A simple electrochemical biosensor for highly sensitive and specific detection of microRNA based on mismatched catalytic hairpin assembly. *Biosens. Bioelectron.* **2015**, *68*, 343–349.

[34] He, Y.; Yang, X.; Yuan, R.; Chai, Y. Q. A novel ratiometric SERS biosensor with one Raman probe for ultrasensitive microRNA detection based on DNA hydrogel amplification. *J. Mater. Chem. B* **2019**, *7*, 2643–2647.

[35] Ke, J. X.; Lu, S.; Li, Z.; Shang, X. Y.; Li, X. J.; Li, R. F.; Tu, D. T.; Chen, Z.; Chen, X. Y. Multiplexed intracellular detection based on dual-excitation/dual-emission upconversion nanoprobes. *Nano Res.* **2020**, *13*, 1955–1961.

[36] Wu, Y.; Xiao, F. B.; Wu, Z. Y.; Yu, R. Q. Novel aptasensor platform based on ratiometric surface-enhanced Raman spectroscopy. *Anal. Chem.* **2017**, *89*, 2852–2858.

[37] Chen, J. Y.; Wu, Y.; Fu, C. C.; Cao, H. Y.; Tan, X. P.; Shi, W. B.; Wu, Z. Y. Ratiometric SERS biosensor for sensitive and reproducible detection of microRNA based on mismatched catalytic hairpin assembly. *Biosens. Bioelectron.* **2019**, *143*, 111619.

[38] Huang, X. L.; Song, J. B.; Yung, B. C.; Huang, X. H.; Xiong, Y. H.; Chen, X. Y. Ratiometric optical nanoprobes enable accurate molecular detection and imaging. *Chem. Soc. Rev.* **2018**, *47*, 2873–2920.

[39] Laing, S.; Gracie, K.; Faulds, K. Multiplex *in vitro* detection using SERS. *Chem. Soc. Rev.* **2016**, *45*, 1901–1918.

[40] Prigodich, A. E.; Randeria, P. S.; Briley, W. E.; Kim, N. J.; Daniel, W. L.; Giljohann, D. A.; Mirkin, C. A. Multiplexed nanoflares: mRNA detection in live cells. *Anal. Chem.* **2012**, *84*, 2062–2066.

[41] Yuan, P. Y.; Mao, X.; Liew, S. S.; Wu, S.; Huang, Y.; Li, L.; Yao, S. Q. Versatile multiplex endogenous RNA detection with simultaneous signal normalization using mesoporous silica nanoquenchers. *ACS Appl. Mater. Interfaces* **2020**, *12*, 57695–57709.

[42] Yeo, D. C.; Wiraja, C.; Paller, A. S.; Mirkin, C. A.; Xu, C. J. Abnormal scar identification with spherical-nucleic-acid technology. *Nat. Biomed. Eng.* **2018**, *2*, 227–238.

[43] Ye, S. J.; Li, X. X.; Wang, M. L.; Tang, B. Fluorescence and SERS imaging for the simultaneous absolute quantification of multiple miRNAs in living cells. *Anal. Chem.* **2017**, *89*, 5124–5130.

[44] Tian, F. R.; Conde, J.; Bao, C. C.; Chen, Y. S.; Curtin, J.; Cui, D. X. Gold nanostars for efficient *in vitro* and *in vivo* real-time SERS detection and drug delivery via plasmonic-tunable Raman/FTIR imaging. *Biomaterials* **2016**, *106*, 87–97.

[45] Wang, L.; Guo, T.; Lu, Q.; Yan, X. L.; Zhong, D. X.; Zhang, Z. P.; Ni, Y. F.; Han, Y.; Cui, D. X.; Li, X. F. et al. Sea-urchin-like Au nanocluster with surface-enhanced Raman scattering in detecting epidermal growth factor receptor (EGFR) mutation status of malignant pleural effusion. *ACS Appl. Mater. Interfaces* **2015**, *7*, 359–369.

[46] Wang, X. S.; Yang, D. P.; Huang, P.; Li, M.; Li, C.; Chen, D.; Cui, D. X. Hierarchically assembled Au microspheres and sea urchin-like architectures: Formation mechanism and SERS study. *Nanoscale* **2012**, *4*, 7766–7772.

[47] Li, G. F.; Yao, Y.; Wang, Z.; Zhao, M.; Xu, J. C.; Huang, L. W.; Zhu, G. M.; Bao, G. J.; Sun, W. S.; Hong, L. et al. Switchable skeletal rearrangement of Dihydroisobenzofuran Acetals with Indoles. *Org. Lett.* **2019**, *21*, 4313–4317.